

Experimental determination of the {111}/{001} surface energy ratio for Pd crystals

Peiyu Chen,^{a),b)} Yakun Gao,^{b)} and Martin R. Castell^{a)}

AFFILIATIONS

Department of Materials, University of Oxford, Parks Road, Oxford, OX1 3PH, United Kingdom

^{a)} Authors to whom correspondence should be addressed: peiyu.chen@materials.ox.ac.uk and martin.castell@materials.ox.ac.uk

^{b)} P.C. and Y.G. contributed equally.

ABSTRACT

Pd crystals grown in ultrahigh vacuum (UHV) on nanostructured SrTiO₃(001) and anatase TiO₂(001) thin film substrates were studied using scanning tunneling microscopy. The crystals have the equilibrium shape of a truncated octahedron with a {111} top facet, {111} and {001} side facets, and a {111} interface. A consistent crystal shape is reached only after annealing the samples in UHV at 450 °C or above. By measuring the top facet dimensions of the equilibrium crystals, we determine the ratio of the surface energies for Pd to be $\gamma_{111}/\gamma_{001} = 0.77 \pm 0.02$.

Palladium (Pd) nanoparticles are widely used in heterogeneous catalysis such as in catalytic converters and in formic acid fuel cells. Their catalytic activity depends on their crystallographic facets which have different atomic structures. For example, when catalyzing the oxidation of formic acid inside a direct formic acid fuel cell, the {001} facets of Pd perform better than the {111} facets. Also, the presence of high-index facets such as {211} and {730} greatly enhance the catalytic activity.¹⁻⁴ The equilibrium shape of a metal nanocrystal depends on its surface energies, which determine the relative stability of the various crystallographic facets. Thus, knowledge of the surface energies of Pd is required to develop a fundamental understanding of the behavior of Pd catalysts.

There have been many theoretical calculations of Pd facet energies using ab-initio methods such as the local density approximation (LDA) and generalized gradient approximation (GGA).⁵⁻¹³ The reported values span a wide range with γ_{111} ranging from 1.15 J m⁻² to 1.92 J m⁻², and γ_{001} ranging from 1.41 J m⁻² to 2.43 J m⁻². In the most recent study, Patra *et al.* determined γ_{111} and γ_{001} for Pd using five different density functionals, from the basic LDA to their most advanced meta-GGA.¹³ They demonstrate that the calculated facet energy strongly depends on the theoretical approach adopted, and their values for either γ_{111} or γ_{001} differ by up to 40% using different approaches. Absolute values of surface energy are notoriously difficult to calculate and even harder to measure experimentally. However, the equilibrium shape of a crystal is determined by the ratios of the facet energies, so from now on we will concentrate on these ratios. The calculated ratio of Pd facet energies, $\gamma_{111}/\gamma_{001}$, falls within the range of 0.82 to 0.88 in the earlier studies.⁵⁻¹²

However, in Patra *et al.*'s five groups of calculations, which we consider to have the most reliable values, the ratios all cluster within the tight range of 0.76 to 0.77. This result is in many ways quite remarkable given the large differences in the absolute facet energy values.

Experimentally, the surface energy of a solid is difficult to measure directly, though the surface energy (or surface tension) in the liquid state has been determined for most elemental metals. Hence, a few surface-energy values for solid Pd have been estimated from its liquid surface tension: $\gamma = 2.00\text{--}2.05 \text{ J m}^{-2}$.^{14–16} For example, Tyson and Miller converted the liquid surface tension into a solid surface energy at the melting temperature by multiplying the surface tension by a factor of 1.18, and then adding a temperature-related factor to derive the surface energy at 0 K, which gave the result $\gamma = 2.00 \text{ J m}^{-2}$.¹⁴ Deriving γ values with this method does not take crystal anisotropy into account, although it has been incorrectly tabulated as “ γ_{111} ” in many publications.^{7,10–12,17} Using a similar approach, Mezey and Giber estimated the solid surface energies for most elemental metals from their enthalpy of atomization, and they obtained $\gamma = 2.04 \text{ J m}^{-2}$ for Pd.¹⁸ Again, this value is not associated with any particular crystal facet.

If surface energies are to be studied from the crystals of a pure metal, the crystals cannot be grown by solution-based synthetic approaches.^{1–4} The resulting crystals are covered by surfactants, and their shapes reflect the surface energies of the surfactant-modified facets. Thus, an adsorbent-free environment such as ultrahigh vacuum (UHV) is required for the crystals to achieve their equilibrium shape as defined by their clean facet energies.

In this letter, we report an experimental study of Pd crystals grown on single crystal strontium titanate (SrTiO_3) substrates (nanostructured or terminated with an anatase film), in which the surface energy ratio of $\gamma_{111}/\gamma_{001}$ is determined. Pd crystals have the face-centered-cubic (fcc) structure, with a truncated octahedral Wulff shape consisting of $\{111\}$ and $\{001\}$ facets, as shown in Fig. 1(a). When Pd crystals are supported on a substrate, they have distinct shapes resulting from different interface crystallographic orientations, depending on the substrate.¹⁹ In our study, the equilibrium Pd crystals have $\{111\}$ top and interface facets, which are both truncated triangles [Fig. 1(b)]. We define the top facet shape by two dimensions: l is the distance from the middle of one $\{001\}$ side facet to the middle of the opposite $\{111\}$ side facet, while s is the width of a $\{001\}$ side facet. Also we call the height of the supported crystal h [Fig. 1(b)].

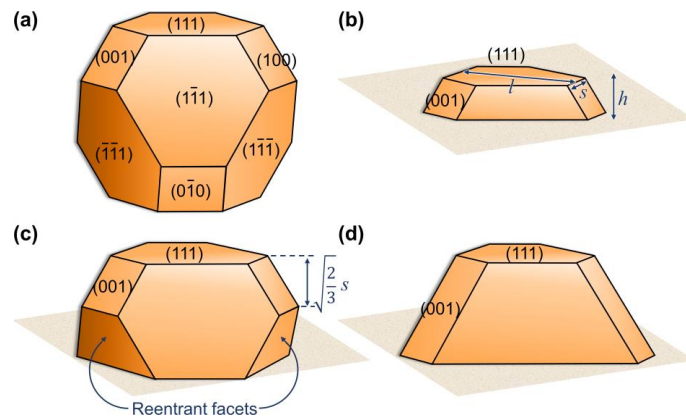


FIG. 1: 3D sketches of Pd crystals: (a) free-standing Wulff shape with $\{111\}$ and $\{001\}$ facets indicated, (b) supported Wulff shape with $h \leq \sqrt{2/3}s$, (c) supported Wulff shape with $h > \sqrt{2/3}s$ showing reentrant facets, and (d) supported growth shape with $h > \sqrt{2/3}s$ without reentrant facets.

When h exceeds $\sqrt{2/3}s$, the supported equilibrium-shaped crystal will form reentrant facets, as drawn in Fig. 1(c). In our study, 74% of the Pd crystals satisfy the condition that $h > \sqrt{2/3}s$, but there is no evidence for the presence of reentrant facets. Instead, the Pd crystals form the growth shape shown in Fig. 1(d), where the $\{001\}$ side facets extend down to the substrate. This was also the case in our previous study of gold crystals grown under similar conditions, in which the formation of growth shapes was explained in terms of kinetic effects during growth.²⁰

In the $(1\bar{1}0)$ cut through the Wulff construction of an fcc crystal, as illustrated in Fig. 2(a), the perpendicular distance of a crystal facet from the Wulff point “O” (h_{hkl}) is proportional to its surface energy (γ_{hkl}).²¹ For this Wulff shape,

$$\frac{\gamma_{111}}{\gamma_{001}} = \frac{h_{111}}{h_{001}}. \quad (1)$$

In Fig. 2(a), the angle $\alpha = 54.74^\circ$ is the acute angle between a $\{111\}$ and a $\{001\}$ plane in an fcc crystal and more precisely $\sin \alpha = \sqrt{\frac{2}{3}}$ and $\cos \alpha = \frac{1}{\sqrt{3}}$. It follows that

$$h_{111} = OA \cdot \sin \alpha = \left(l \cdot \cos \alpha + \frac{s}{2} \right) \cdot \sin \alpha = \frac{\sqrt{2}}{3} l + \frac{s}{\sqrt{6}} \quad (2)$$

$$h_{001} = l \cdot \sin \alpha = \sqrt{\frac{2}{3}} l. \quad (3)$$

Substituting equations (2) and (3) into equation (1) gives

$$\frac{\gamma_{111}}{\gamma_{001}} = \frac{1}{\sqrt{3}} + \frac{s}{2l}. \quad (4)$$

Alternatively, equation (4) can also be derived analytically by minimizing the total surface energy (E) for a given volume:

$$E = \gamma_{001}A_{001} + \gamma_{111}A_{111}, \quad (5)$$

where A_{001} and A_{111} are facet areas of the crystal with the geometry in Fig. 1(a).

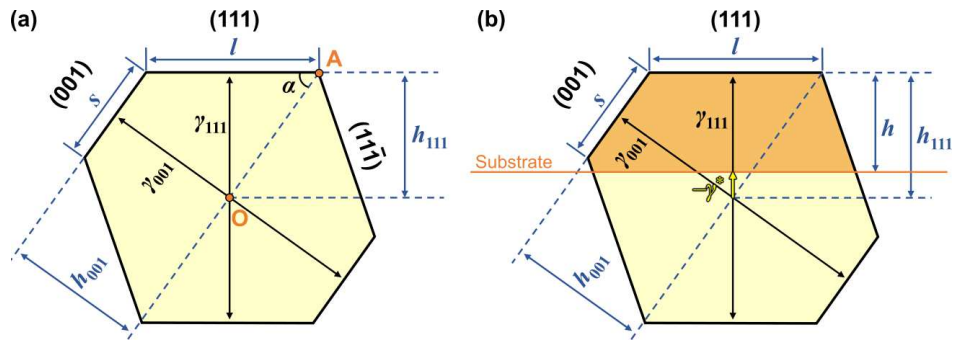


FIG. 2: $(1\bar{1}0)$ cut through the (a) Wulff and (b) Winterbottom constructions of a Pd crystal.

Equation (4) also applies to the substrate-supported Wulff crystals in Figs. 1(b) and 1(c), the heights of which are predicted by the Winterbottom construction,²² also known as the Wulff-Kaisheff theorem.²³ This is depicted in Fig. 2(b), where an extra energy term γ^* is included at the crystal-substrate interface, defined as $\gamma^* = \gamma_{\text{interface}} - \gamma_{\text{substrate}}$ (or $\gamma_i - \gamma_s$).²⁴ According to the Winterbottom construction,²²

$$\frac{-\gamma^*}{\gamma_{111}} = \frac{h_{111} - h}{h_{111}}. \quad (6)$$

Combining equation (6) with equations (1) and (3) results in

$$\gamma^* = \sqrt{\frac{3}{2}} \frac{h}{l} \gamma_{001} - \gamma_{111}. \quad (7)$$

Equation (7) applies to Wulff shapes with any height, i.e., whether $h \leq \sqrt{2/3}s$ [Fig. 1(b)] or $h > \sqrt{2/3}s$ [Fig. 1(c)].

Equation (7) can also be calculated by minimizing the total surface/interface energy (E) of a crystal with a given volume:

$$E = \gamma_{001}A_{001} + \gamma_{111}A_{111} + \gamma^*A_i, \quad (8)$$

where A_i is the crystal–substrate interfacial area. The Wulff shapes drawn in Fig. 1(b) ($h \leq \sqrt{2/3}s$) and Fig. 1(c) ($h > \sqrt{2/3}s$) have different geometries. Their area terms are different and so are the expressions for their total energies (E), but minimizing E for both geometries leads to equation (7). Equations (4) and (7) describe the key relationships for the Wulff shapes in Figs. 1(b) and 1(c). They relate the crystal surface/interface energies (γ_{111} , γ_{001} , and γ^*) to the crystal dimensions (l , s , and h).

Our Pd crystals often adopt the growth shape shown in Fig. 1(d) where the Winterbottom construction does not apply, but we can still derive the energy–dimension relationships by minimizing the total energy E , described by equation (8). Because the growth shape in Fig. 1(d)

has the same geometry as the Wulff shape in Fig. 1(b), they share the same expression for the total energy E , and minimizing E for this geometry still results in equations (4) and (7), regardless of the magnitude of h . Therefore, these equations apply to all the supported crystal shapes in Fig. 1. In this study, we use equation (4), which relates the s/l ratio measured from our Pd crystals, to the surface energy ratio of $\gamma_{111}/\gamma_{001}$.

As an additional comment, when $h > \sqrt{2/3}s$, the growth shape [Fig. 1(d)] is higher in energy than the Wulff shape [Fig. 1(c)]. We calculated the small energy difference between these shapes in our previous study on gold crystals.²⁰ As an example, in our current study, for a relatively high crystal, when the Wulff point is in the plane of the substrate ($\gamma^* = 0$), the surface/interface energy of the growth shape is only around 3% greater than for the equilibrium shape with reentrant facets.

In this study, SrTiO₃ substrates doped with Nb at 0.5% by weight and epi-polished on (001) facets were supplied by PI-KEM, U.K. On SrTiO₃(001), we prepared two surfaces: the (6 × 2) nanostructured surface,^{25–27} and the anatase TiO₂(001) epitaxial thin film structure with a (1 × 4) reconstruction.^{28,29} Pd was then deposited from an *e*-beam evaporator using 99.95% pure Pd rods supplied by Goodfellow, U.K. to form a coverage of 0.5–1.3 monolayers, followed by post annealing in UHV. The Pd crystals were imaged by scanning tunneling microscopy (STM) (JEOL JSTM 4500s model, base pressure 10^{–8} Pa). STM images were processed by *Gwyddion* and *WSxM*.³⁰

Figure 3 shows 3D-rendered STM images of some of the supported Pd crystals. These crystals only

reach a consistent shape after post annealing at ~ 450 °C or above. For example, the crystals in Fig. 3(a) were grown and post-annealed at 300 °C for 30 min. Most crystals have $\{111\}$ bases but two crystals with $\{110\}$ bases are also seen. They adopt a “hut” shape,¹⁹ which is a metastable orientation that can nucleate randomly and is then not able to convert into the equilibrium $\{111\}$ orientation due to kinetic limitations at 300 °C. Even the truncated triangular crystals in Fig. 3(a) vary in shape – some are more pointed and some are elongated. In contrast, when the crystals are post-annealed at 450–650 °C, they exhibit a consistent top-facet shape across a range of widths ($l = 3\text{--}9$ nm), as shown by the examples in Fig. 3(b). Figure 3 presents a mixture of Pd crystals on the two different substrates. The equilibrium top-facet shape is found to be independent of the substrate, since the s/l ratio is solely determined by the $\gamma_{111}/\gamma_{001}$ ratio of Pd according to equation (4).

We observed that the Pd crystals can become encapsulated by a TiO_x layer migrating from the substrates when heated at ~ 600 °C or above. The encapsulated crystals are distinguishable from bare crystals, as their STM images display clear moiré patterns on their top facets.³¹ The encapsulation alters the equilibrium shape of the Pd crystals, so for the purpose of calculating the $\gamma_{111}/\gamma_{001}$ ratio in this study, we only present and analyze bare Pd crystals in Figs. 3 and 4.

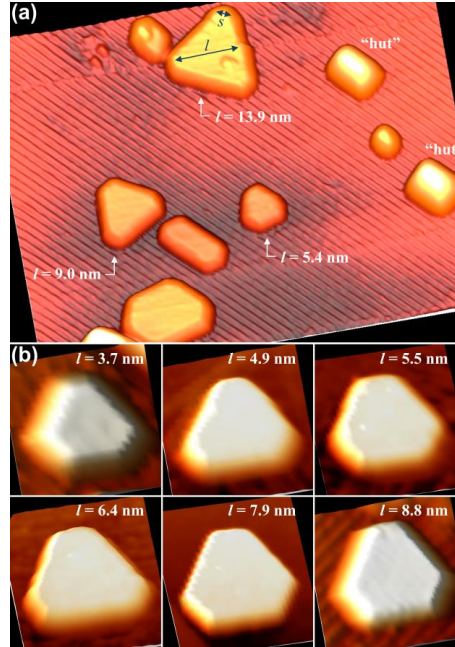


FIG. 3: Pd crystals of various sizes, where the top facet width l is labeled for all three-fold symmetric $\{111\}$ -oriented crystals: (a) nucleated, grown, and post-annealed at 300 °C for 30 min ($V_s = 1.7$ V, $I_t = 0.27$ nA) and (b) nucleated, grown, and post-annealed at 450–650 °C for 60 min ($V_s = 1.7$ –2.0 V, $I_t = 0.17$ –0.30 nA). In (a), two non-equilibrium “hut”-shaped $\{110\}$ oriented crystals are also indicated. The Pd crystals are supported on anatase substrates in (a) and in the first ($l = 3.7$ nm) and last ($l = 8.7$ nm) panels in (b). Other crystals in (b) are supported on nanostructured $\text{SrTiO}_3(001)$ substrates.

Figure 4 shows the plot of the s/l ratio vs l for Pd crystals. We only measured the dimensions of crystals that have a flat top facet and are three-fold rotationally symmetric, which is the minimum requirement for an equilibrium shape. For the self-similar crystals that formed at 450 °C or above, their s/l ratios are both found to center around the same constant on the two different substrates (red triangles and orange squares), with a value of $s/l = 0.39 \pm 0.04$. Since these data points do not show any detectable change with increasing width l , this implies that these crystals have reached

their equilibrium geometry. On the other hand, the s/l ratio for Pd crystals annealed at 300 °C on anatase decreases with increasing l (green dots), from the equilibrium value of 0.39 towards ~0.20 as l approaches ~18 nm.

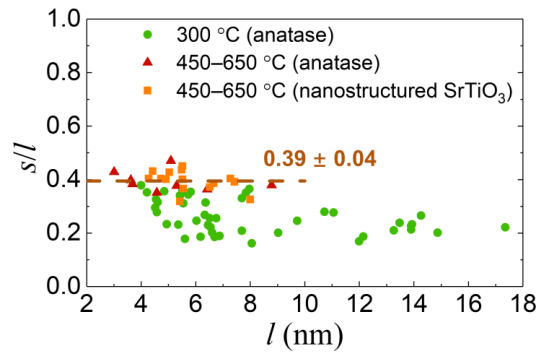


FIG. 4: s/l ratio plotted against l for Pd crystals post-annealed at different temperatures on anatase thin film and nanostructured SrTiO₃(001) substrates.

The change in the relative dimensions of the Pd crystals following higher temperature annealing can be explained via kinetics. During the ripening process the Pd atoms diffuse to a growing crystal via the substrate and initially attach at the base of the crystals. This means that at low annealing temperatures (300 °C) the crystals are relatively flat. Higher anneal temperatures (450–650 °C) are required for the atoms within the Pd crystal to diffuse sufficiently to achieve the equilibrium shape. As an indication of the crystal sizes, the average height for the 300 °C-annealed crystals is 2.05 ± 0.30 nm, and that for the 450–650 °C-annealed crystals is 2.56 ± 0.80 nm.

Using equation (4), the equilibrium s/l value of 0.39 ± 0.04 can be converted into a $\gamma_{111}/\gamma_{001}$ ratio of 0.77 ± 0.02 . This lies within the 0.76–0.88 range of theoretically predicted values reported

in the literature,^{5–13} and it agrees particularly well with Patra *et al.*'s results of 0.76–0.77.¹³

Although there are many experimental STM studies that reveal the {111} top facets of Pd crystals,^{19,24,32–36} only a few have used the images to explicitly analyze the $\gamma_{111}/\gamma_{001}$ ratio.^{24,36} For example, Ahmadi *et al.* obtained a ratio of $\gamma_{111}/\gamma_{001} = 0.89 \pm 0.06$.³⁶ However, this is an unreliable value because it was calculated from the average of a very wide spread of {001} to {111} area ratios ranging from 0.15 to 1.12, and therefore cannot be considered to represent thermodynamic equilibrium. In Hansen *et al.*'s work, Pd crystals were grown on an Al₂O₃ thin film substrate in UHV at room temperature and they report a $\gamma_{111}/\gamma_{001}$ ratio of 0.74 ± 0.03 .²⁴ Their Pd crystals show morphologies of which most have not reached a three-fold symmetric shape due to kinetic limitations. Their measurements of the crystal top facets is equivalent to an s/l ratio of 0.33 ± 0.06 . This is lower than our equilibrium value of 0.39 ± 0.04 and is associated with a larger standard deviation, similar to the behavior of our green dots (300 °C annealing temperature) in Fig. 4. We believe that the lack of kinetic energy is the reason why both our 300 °C-annealed crystals and those of Hansen *et al.*'s room-temperature grown crystals result in non-equilibrium structures.³⁷

In summary, we have grown Pd crystals in UHV on oxide substrates, with truncated triangular {111} top and base facets and {001} and {111} side facets. The Pd crystals reach their equilibrium shapes after being annealed at ~450 °C or above, where they have a constant s/l ratio of 0.39 ± 0.04 . This is used to calculate a $\gamma_{111}/\gamma_{001}$ ratio of 0.77 ± 0.02 . It is found that Pd crystals annealed at lower temperatures such as 300 °C have lower values of s/l and a broader spread of values because kinetic

limitations prevent the thermodynamic equilibrium shape from being achieved. Similar carefully executed experiments could be used to determine the surface energy ratios of other catalytically interesting metals in UHV.

ACKNOWLEDGEMENTS

This work was supported by EPSRC grants EP/K032518/1 and EP/M015173/1. The authors would like to thank Chris Spencer (JEOL U.K.) for technical support and the China Scholarship Council (CSC) for financial support.

DATA AVAILABILITY

The data that support the findings of this study are available within the article.

REFERENCES

- ¹ X. Huang, S. Tang, H. Zhang, Z. Zhou, and N. Zheng, J. Am. Chem. Soc. **131**, 13916 (2009).
- ² M. Jin, H. Zhang, Z. Xie, and Y. Xia, Angew. Chemie - Int. Ed. **50**, 7850 (2011).
- ³ M. Jin, H. Zhang, Z. Xie, and Y. Xia, Energy Environ. Sci. **5**, 6352 (2012).

This is the author's peer reviewed, accepted manuscript. However, the online version of record will be different from this version once it has been copyedited and typeset.

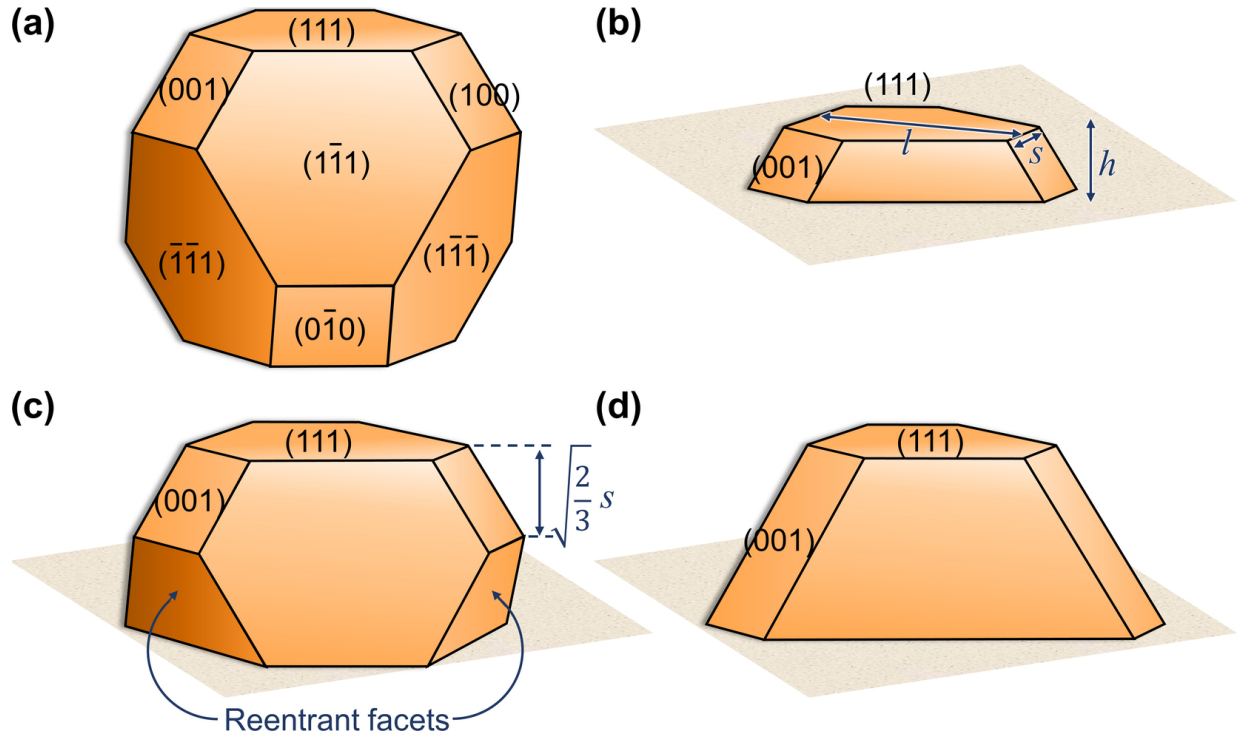
PLEASE CITE THIS ARTICLE AS DOI: 10.1063/5.0022879

- ⁴ S. Il Choi, J.A. Herron, J. Scaranto, H. Huang, Y. Wang, X. Xia, T. Lv, J. Park, H.C. Peng, M. Mavrikakis, and Y. Xia, *ChemCatChem* **7**, 2077 (2015).
- ⁵ H.L. Skriver and N.M. Rosengaard, *Phys. Rev. B* **7** 157 (1992).
- ⁶ M. Methfessel, D. Hennig, and M. Scheffler, *Phys. Rev. B* **46**, 4816 (1992).
- ⁷ L. Vitos, A. V. Ruban, H.L. Skriver, and J. Kollár, *Surf. Sci.* **411**, 186 (1998).
- ⁸ J.M. Zhang, F. Ma, and K.W. Xu, *Appl. Surf. Sci.* **229**, 34 (2004).
- ⁹ T.M. Trimble and R.C. Cammarata, *Surf. Sci.* **602**, 2339 (2008).
- ¹⁰ N.E. Singh-Miller and N. Marzari, *Phys. Rev. B* **80**, 235407 (2009).
- ¹¹ B. Fu, W. Liu, and Z. Li, *Appl. Surf. Sci.* **256**, 6899 (2010).
- ¹² J. Wang and S.Q. Wang, *Surf. Sci.* **630**, 216 (2014).
- ¹³ A. Patra, J.E. Bates, J. Sun, and J.P. Perdew, *Proc. Natl. Acad. Sci. U. S. A.* **114**, E9188 (2017).
- ¹⁴ W.R. Tyson and W.A. Miller, *Surf. Sci.* **62**, 267 (1977).
- ¹⁵ A.R. Miedema, *Zeitschrift Für Met.* **69**, 287 (1978).
- ¹⁶ F.R. de Boer, R. Boom, W.C.M. Mattens, A.R. Miedema, and A.K. Niessen, *Cohesion in Metals : Transition Metal Alloys* (North-Holland, Amsterdam, 1988).
- ¹⁷ J.L.F. Da Silva, C. Stampfl, and M. Scheffler, *Surf. Sci.* **600**, 703 (2006).
- ¹⁸ L.Z. Mezey and J. Giber, *Jpn. J. Appl. Phys.* **21**, 1569 (1982).
- ¹⁹ F. Silly and M.R. Castell, *Phys. Rev. Lett.* **94**, 046103 (2005).
- ²⁰ P. Chen, K. Murugappan, and M.R. Castell, *Phys. Chem. Chem. Phys.* **22**, 4416 (2020).
- ²¹ G.Z. Wulff, *Kryst. Miner.* **34**, 449 (1901).
- ²² W.L. Winterbottom, *Acta Metall.* **15**, 303 (1967).

- ²³ R. Kaishew, *Arbeitstagung Festkörper Physik* (Dresden, 1952).
- ²⁴ K.H. Hansen, T. Worren, S. Stempel, E. Lægsgaard, M. Bäumer, H.-J. Freund, F. Besenbacher, and I. Stensgaard, *Phys. Rev. Lett.* **83**, 4120 (1999).
- ²⁵ D.S. Deak, F. Silly, D.T. Newell, and M.R. Castell, *J. Phys. Chem. B* **110**, 9246 (2006).
- ²⁶ H.L. Marsh, D.S. Deak, F. Silly, A.I. Kirkland, and M.R. Castell, *Nanotechnology* **17**, 3543 (2006).
- ²⁷ M.S.J. Marshall, A.E. Becerra-Toledo, D.J. Payne, R.G. Egde, L.D. Marks, and M.R. Castell, *Phys. Rev. B* **86**, 125416 (2012).
- ²⁸ F. Silly and M.R. Castell, *Appl. Phys. Lett.* **85**, 3223 (2004).
- ²⁹ M.S.J. Marshall and M.R. Castell, *Phys. Rev. Lett.* **102**, 146102 (2009).
- ³⁰ I. Horcas, R. Fernández, J.M. Gómez-Rodríguez, J. Colchero, J. Gómez-Herrero, and A.M. Baro, *Rev. Sci. Instrum.* **78**, 013705 (2007).
- ³¹ F. Silly and M.R. Castell, *J. Phys. Chem. B* **109**, 12316 (2005).
- ³² K. Højrup Hansen, Šljivančanin, E. Lægsgaard, F. Besenbacher, and I. Stensgaard, *Surf. Sci.* **505**, 25 (2002).
- ³³ F. Silly, A.C. Powell, M.G. Martin, and M.R. Castell, *Phys. Rev. B* **72**, 165403 (2005).
- ³⁴ C. Nörenberg and M.R. Castell, *Surf. Sci.* **601**, 4438 (2007).
- ³⁵ M. Ahmadi, F. Behafarid, C. Holse, J.H. Nielsen, and B. Roldan Cuenya, *J. Phys. Chem. C* **119**, 29178 (2015).
- ³⁶ M. Ahmadi, F. Behafarid, and B.R. Cuenya, *Nanoscale* **8**, 11635 (2016).
- ³⁷ L.D. Marks and L. Peng, *J. Phys. Condens. Matter* **28**, 53001 (2016).

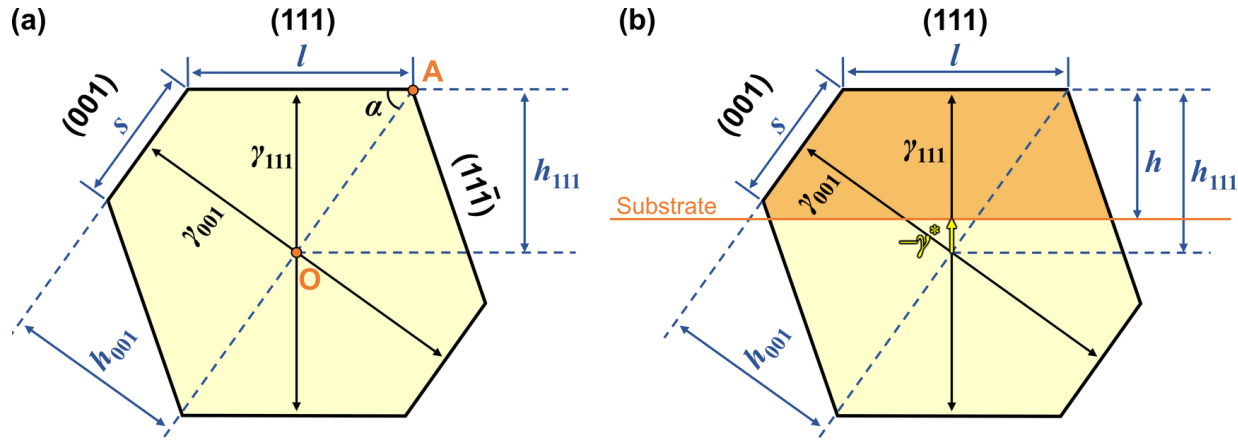
This is the author's peer reviewed, accepted manuscript. However, the online version of record will be different from this version once it has been copyedited and typeset.

PLEASE CITE THIS ARTICLE AS DOI: 10.1063/5.0022879



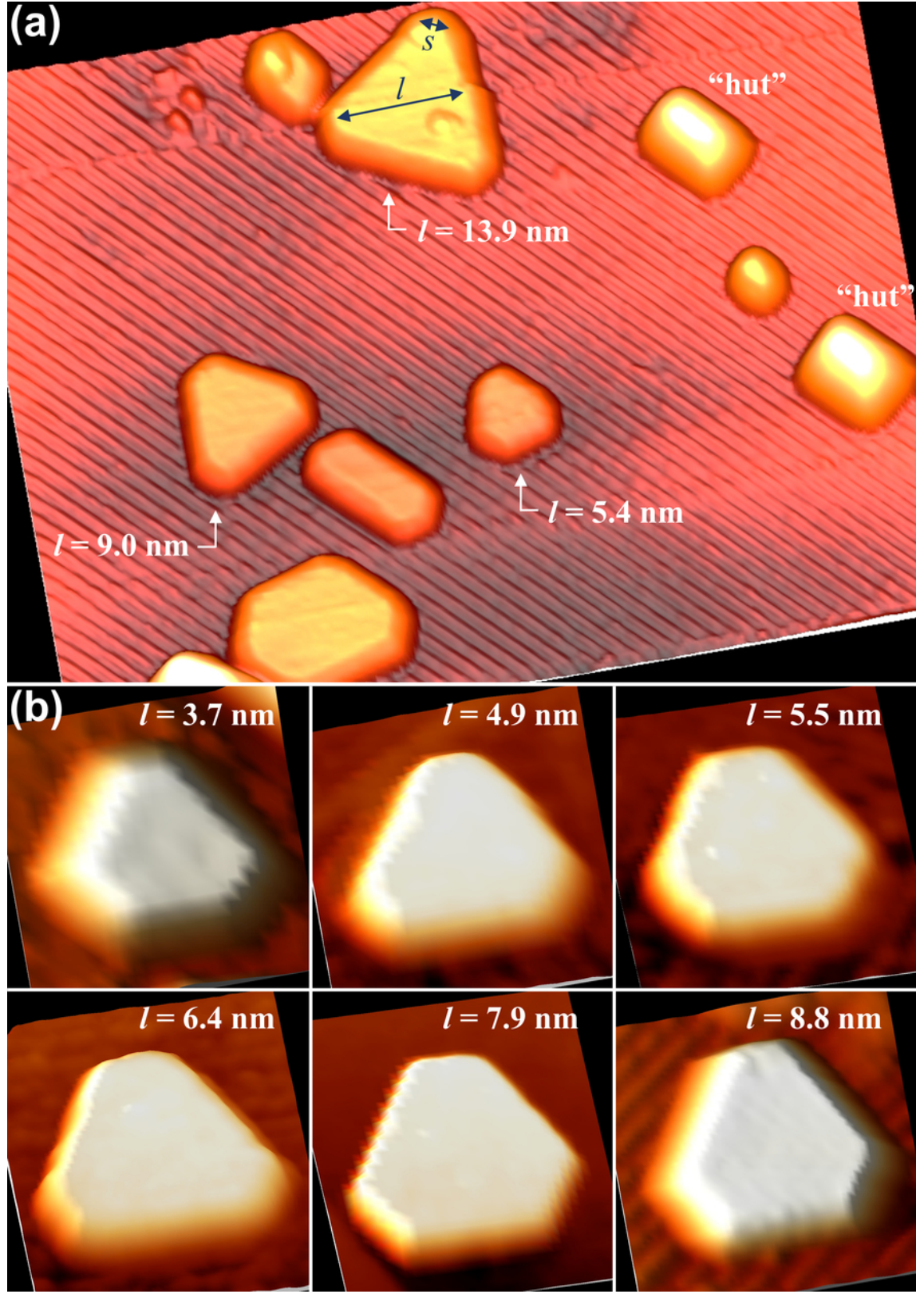
This is the author's peer reviewed, accepted manuscript. However, the online version of record will be different from this version once it has been copyedited and typeset.

PLEASE CITE THIS ARTICLE AS DOI: 10.1063/5.0022879



This is the author's peer reviewed, accepted manuscript. However, the online version of record will be different from this version once it has been copyedited and typeset.

PLEASE CITE THIS ARTICLE AS DOI: 10.1063/5.0022879



This is the author's peer reviewed, accepted manuscript. However, the online version of record will be different from this version once it has been copyedited and typeset.

PLEASE CITE THIS ARTICLE AS DOI: 10.1063/5.0022879

